AFRL-AFOSR-JP-TR-2022-0013

Electromagnetic Energy Deposition During M-I-T coupling

Horvath, Ildiko
THE UNIVERSITY OF QUEENSLAND
UNIVERSITY OF QUEENSLAND
BRISBANE, , 4072
AUS

01/09/2022
Final Technical Report

Air Force Research Laboratory
Air Force Office of Scientific Research
Asian Office of Aerospace Research and Development
Unit 45002, APO AP 96338-5002

REPORT DOCUMENTATION PAGE

PLEASE DO NOT RETURN YOUR FORM TO THE ABOVE ORGANIZATION.

1. REPORT DATE	**2. REPORT TYPE**	**3. DATES COVERED**	
20220109	Final	**START DATE** 20190830	**END DATE** 20210829

4. TITLE AND SUBTITLE
Electromagnetic Energy Deposition During M-I-T coupling

5a. CONTRACT NUMBER	**5b. GRANT NUMBER**	**5c. PROGRAM ELEMENT NUMBER**
FA2386-19-1-4081		61102F
5d. PROJECT NUMBER	**5e. TASK NUMBER**	**5f. WORK UNIT NUMBER**

6. AUTHOR(S)
Ildiko Horvath

7. PERFORMING ORGANIZATION NAME(S) AND ADDRESS(ES)
THE UNIVERSITY OF QUEENSLAND
UNIVERSITY OF QUEENSLAND
BRISBANE 4072
AUS

8. PERFORMING ORGANIZATION REPORT NUMBER

9. SPONSORING/MONITORING AGENCY NAME(S) AND ADDRESS(ES)	**10. SPONSOR/MONITOR'S ACRONYM(S)**	**11. SPONSOR/MONITOR'S REPORT NUMBER(S)**
AOARD UNIT 45002 APO AP 96338-5002	AFRL/AFOSR IOA	AFRL-AFOSR-JP-TR-2022-0013

12. DISTRIBUTION/AVAILABILITY STATEMENT
A Distribution Unlimited: PB Public Release

13. SUPPLEMENTARY NOTES

14. ABSTRACT
The main objective of this project is to investigate solar wind (SW), magnetospheric (M), ionospheric (I), and thermospheric (T) processes in order to better understand how the electromagnetic energy deposited from the coupled SW-M system impacted the coupled I-T system. To fulfill the main objective, we investigated both i) the electromagnetic and geophysical processes occurring in the coupled SW-M system and ii) the resultant topside ionospheric and thermospheric responses. The specific main aims of the research are to investigate 1) solar wind, Interplanetary Magnetic Field (IMF) and Interplanetary Electric Field (IEF) variations, 2) dayside magnetopause and nightside magnetotail reconnection events supplying the electromagnetic energy, 3) thermospheric responses, and 4) how the coupled high-latitude M-I-T system impacts the auroral and subauroral regions.

15. SUBJECT TERMS

16. SECURITY CLASSIFICATION OF:			**17. LIMITATION OF ABSTRACT**	**18. NUMBER OF PAGES**
a. REPORT	**b. ABSTRACT**	**c. THIS PAGE**		
U	U	U	SAR	16

19a. NAME OF RESPONSIBLE PERSON	**19b. PHONE NUMBER** *(Include area code)*
TONY KIM	315-227-7008

Section 2: Technical Report

2 Accomplishments

2.1 Research Objectives

The main objective of this project is to investigate solar wind (SW), magnetospheric (M), ionospheric (I), and thermospheric (T) processes in order to better understand how the electromagnetic energy deposited from the coupled SW-M system impacted the coupled I-T system. To fulfill the main objective, we investigated both i) the electromagnetic and geophysical processes occurring in the coupled SW-M system and ii) the resultant topside ionospheric and thermospheric responses. The specific main aims of the research are to investigate 1) solar wind, Interplanetary Magnetic Field (IMF) and Interplanetary Electric Field (IEF) variations, 2) dayside magnetopause and nightside magnetotail reconnection events supplying the electromagnetic energy, 3) thermospheric responses, and 4) how the coupled high-latitude M-I-T system impacts the auroral and subauroral regions.

This project's scientific approach is unique since it specifies the flow channels developed in the polar cap and at auroral and subauroral latitudes. It also applies the flow channel-related information and the flow channel-associated magnetospheric and ionospheric phenomena to the investigation of the coupled M-I-T system. Since electrodynamic M-I-T coupling is present during both magnetically active and quiet times, the project includes the investigation of a series of storms/substorms and magnetically moderate-quiet time periods. Regarding the investigations of the various subauroral flow channel development, this project considers the most up to date fast-time theory put forward by recent studies (Mishin, 2013; Mishin et al., 2017; Mishin & Streltsov, 2021). This project also relates the various events of interest to specific science problems reported in the literature. In this way, the project results can contribute to and add directly to recent investigations, so the new results obtained can be integrated into the recent research efforts of MURI and AFRL.

This project's technical approach is to utilize 1) ACE data to investigate solar wind, IMF and IEF variations triggering dayside magnetopause and nightside magnetotail reconnection events, 2) Polar/Cluster/THEMIS/MMS satellite measurements to investigate i) dayside magnetopause and ii) nightside magnetotail reconnection events supplying the electromagnetic energy and iii) Kelvin-Helmholtz (K-H) surface waves rippling the plasma sheet and facilitating dayside magnetopause reconnection within the K-H vortices, 3) DMSP spacecraft measurements to observe topside ionospheric responses and energy deposition quantified by the Poynting flux that was computed based on the methodology of Huang et al. (2014), and CHAMP satellite data to observe thermospheric responses.

According to the work plan, the project started with the investigation of M-I-T coupling occurring during a series of magnetically intense storms (i.e. great storms and superstorms). Then, the energy deposition is most intense and both the ionospheric flow channels and the thermospheric localized neutral density increases/depletions are best developed and thus, the SW-M-I-T coupling processes are most pronounced and easiest to recognize. The improved understanding obtained aided the investigations of less intense storms when the SW-M-I-T coupling processes are less pronounced.

References:

Huang, C. Y., & Burke, W. J. (2004). Transient sheets of field-aligned current observed by DMSP during the main phase of a magnetic superstorm. *Journal of Geophysical Research, 109(A6),* A06303. https://doi.org/10.1029/2003JA010067

Mishin, E. V. (2013). Interaction of substorm injections with the subauroral geospace: 1. Multispacecraft observations of SAID. *Journal of Geophysical Research: Space Physics, 118(9),* 5782-5796. https://doi.org/10.1002/jgra.50548

Mishin, E., Nishimura, Y., & Foster, J. (2017). SAPS/SAID revisited: A causal relation to the substorm current wedge. *Journal of Geophysical Research: Space Physics, 122(8),* 8516-8535. https://doi.org/10.1002/2017JA024263

Mishin, E., & Streltsov, A. (2021). Mesoscale and Small-Scale Structure of the Subauroral Geospace. In Huang, C., &. Lu, G. (Eds.), *Space Physics and Aeronomy Collection Volume 3:* Ionosphere Dynamics and Applications, Geophysical Monograph Series (Vol 260, pp.135-154) Washington DC: American Geophysical Union. https://doi.org/10.1002/9781119815617.ch8

2..2 Details of accomplishments during this project

2.2.1 M-I-T coupling occurring during great/superstorms at subauroral latitudes on the duskside

Investigating M-I-T coupling occurring during magnetically intense storms, when energy deposition is most intense and the subauroral flows are strongest, and the localized neutral density increases/depletions are best developed, provides an excellent opportunity to better understand the underlying solar wind, magnetospheric, ionospheric, and thermospheric processes (i.e. SW-M-I-T coupling) that are most pronounced.

We investigated the 24-25 September 1998 great storm, the 7-8 November 2004 superstorm, and the 21-22 January 2005 moderate storm that showed superstorm characteristics (Kozyra et al., 2014). Our results reported in the journal article of Horvath & Lovell (2021a) reveal the repeated development of a complex subauroral flow channel structure during these storms, as these superstorms provided favorable conditions for their development. These complex subauroral flow channel structures were created by the Double-Peak Sub-Auroral Ion Drifts (DSAID; He et al., 2016), Abnormal Sub-Auroral Ion Drifts (ASAID; Voiculescu & Roth, 2008), and Sub-Auroral Polarization Streams (SAPS; Foster & Burke, 2002). The combined DSAID-ASAID flow channel structure appeared as a northern-hemisphere—southern-hemisphere conjugate and transient feature (see Figures 1-2) that declined to a DSAID feature. The DSAID component developed due to the enhancement of ↓R2-FACs (He et al., 2016), as the trapped ring current particles formed a double spatial pressure peak structure generating two sets of ↓R2 FACs and two large poleward-directed subauroral E fields (Wei et al., 2019). In good agreement with the study of Wei et al. (2019), this double pressure peak ring current structure was seen, during or just before the DSAID-ASAID detections, in the LANL-detected 225 keV proton density data (see Figure 1d) representing the terrestrial ring current's plasma density population (Maurice et al., 1998). Thus, this study's LANL detections provide additional observational evidence (for the first time) of the double peak ring current structure leading to DSAID development, as reported by Wei et al. (2019).

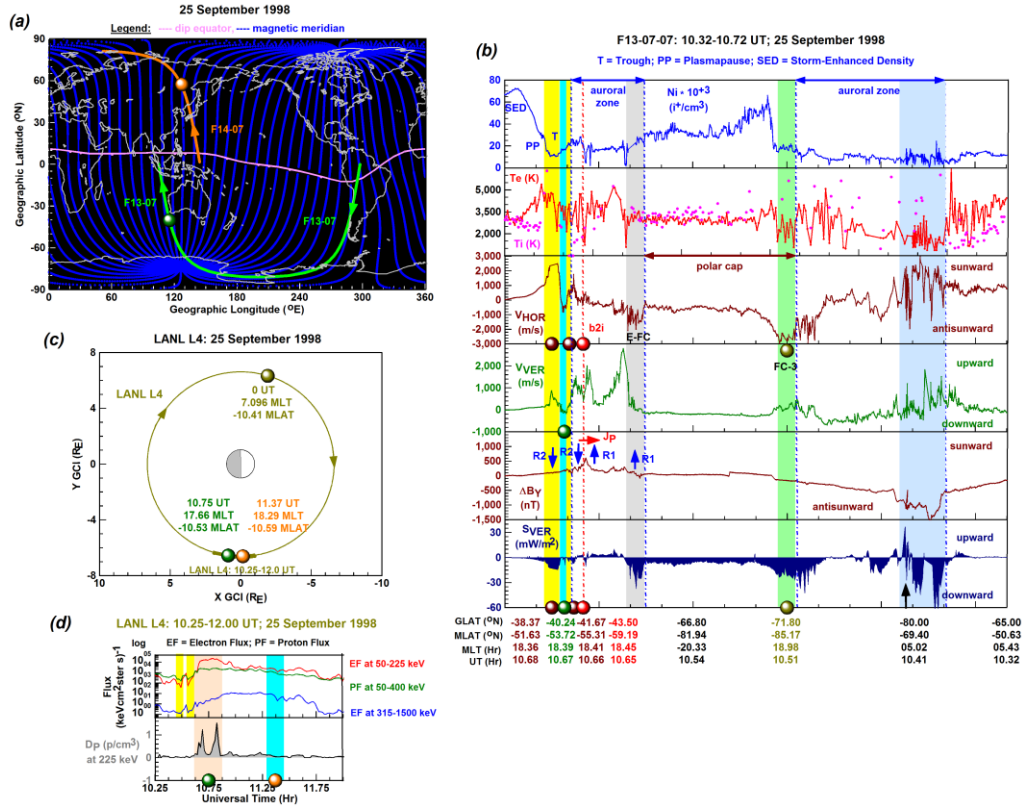

Figure 1: (a) The global map shows the DMSP ground tracks and the northern-southern conjugate DSAID-ASAID features' locations. (b) The DMSP line plot sets depict the southern DSAID-ASAID and their plasma environment. (c) The LANL orbit plot shows the orbit section covered during the DSAID-ASAID detections. (d) The LANL-detected 225 keV proton density time series depicts the signature of double ring current flow during the southern DSAID-ASAID detection.

The ASAID component developed due to plasma sheet rippling (observed by Polar; see Figures 2f-g) forming a magnetospheric cold-plasma-ripple—hot-ring-current interface leading to ASAID development (Horvath & Lovell, 2019a, 2019b). Furthermore, we provided further observational evidence that ASAID development was triggered by plasma sheet rippling and during the operation of the substorm current wedge 2-loop (SCW2L) system. Forming these complex DSAID-ASAID features during the storms investigated, the individual DSAID and ASAID components appeared together since plasma sheet rippling occurred during DSAID development: DSAID occurred during the later stage of plasma sheet rippling triggering ASAID development.

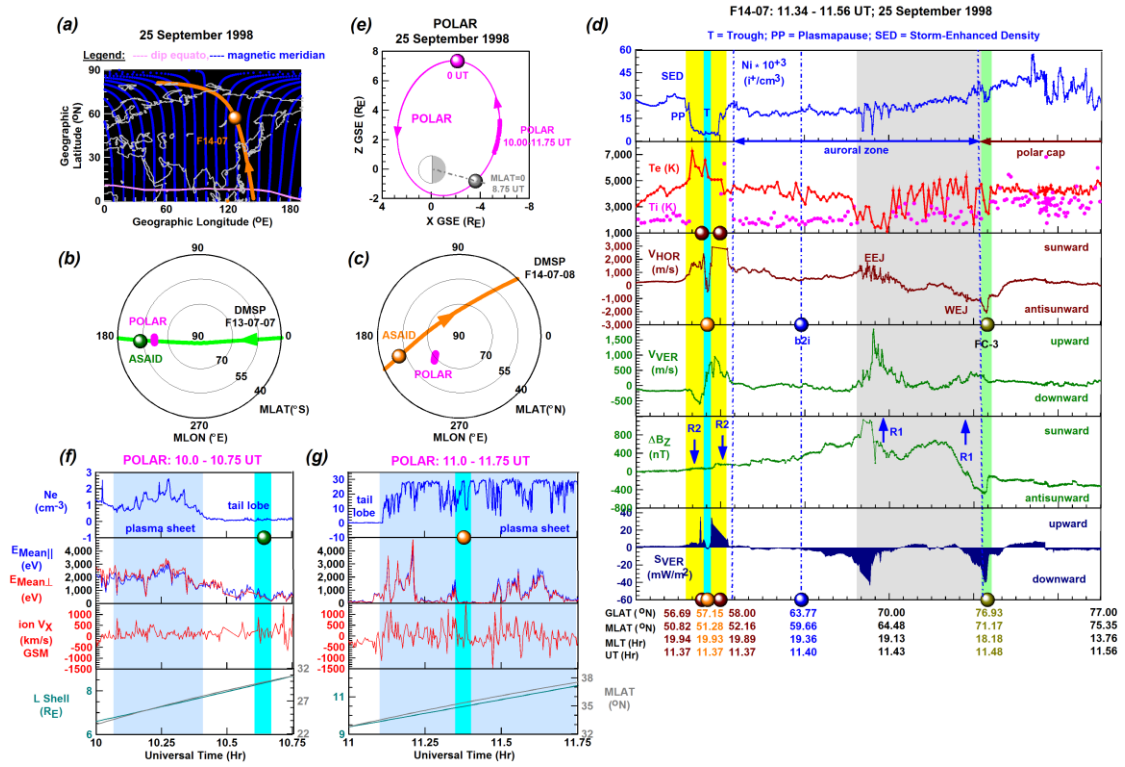

Figure 2: (a)-(c) The various maps show the locations of the northern (in orange) and southern (in green) DSAID-ASAID features. (d) The DMSP line plot sets depict the northern DSAID-ASAID and their plasma environment. (e) The Polar orbit plot shows the location of plasma sheet detection. (f)-(g) The Polar time series depict rippled plasma sheet.

We provided observational evidence in Horvath & Lovell (2021b) that the net subauroral westward currents became enhanced and the net zonal (E- and F-region) drift created a deep O^+ trough that deepened the midlatitude trough and led to amplified SAPS flows via positive feedback mechanisms (see Figure 3).

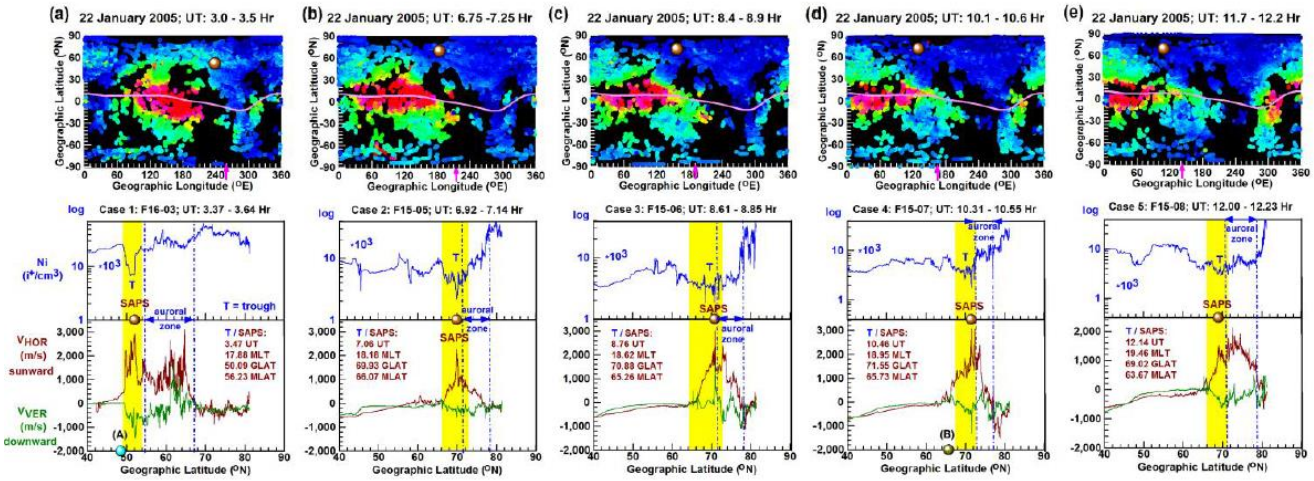

Figure 3: (a)-(e) The GPS TEC maps depict the low total electron content (TEC) at the trough location (marked in each map as symbol dot in dark orange). The DMSP Ni and cross-track drift plots show the trough and the amplified SAPS flows and downward drifts within the trough (marked in each figure as shaded interval in yellow).

2.2.2 M-I-T coupling occurring during great/superstorms at equatorial and low latitudes

We further investigated the 21 January 2005 moderate storm, which showed superstorm characteristics (Kozyra et al., 2014), and reported new results in the journal article of Horvath & Lovell (2021b). We focused on the prompt penetration electric field (PPEF) effects in the American sector, the Rayleigh-Taylor (R-T) instability driven polarization electric (E) field effects in the African sector, and the disturbance dynamo electric field (DDEF) effects in the Northern Hemisphere. We studied how these E field effects impacted the Equatorial Ionization Anomaly (EIA) and underlying forward fountain, the midlatitude trough, and SAPS. Our results show that strong M-I-T coupling was present at equatorial and subauroral latitudes (see Figure 4). At equatorial latitudes and during an evening pre-reversal enhancement (PRE)-like scenario, the activated Rayleigh-Taylor (R-T) instability mechanisms led to the development of supersonic bubbles drifting upward and westward (see Figures 4c-d). Since supersonic bubbles are characteristics of superstorms, their detections further verify the 21 January 2005 moderate storm's turbulent and superstorm nature reported by Kozyra et al. (2014). At subauroral latitudes, SAPS flows developed and became amplified during the anti-Solar quiet (anti-Sq) current system's operation due to the positive feedback mechanisms.

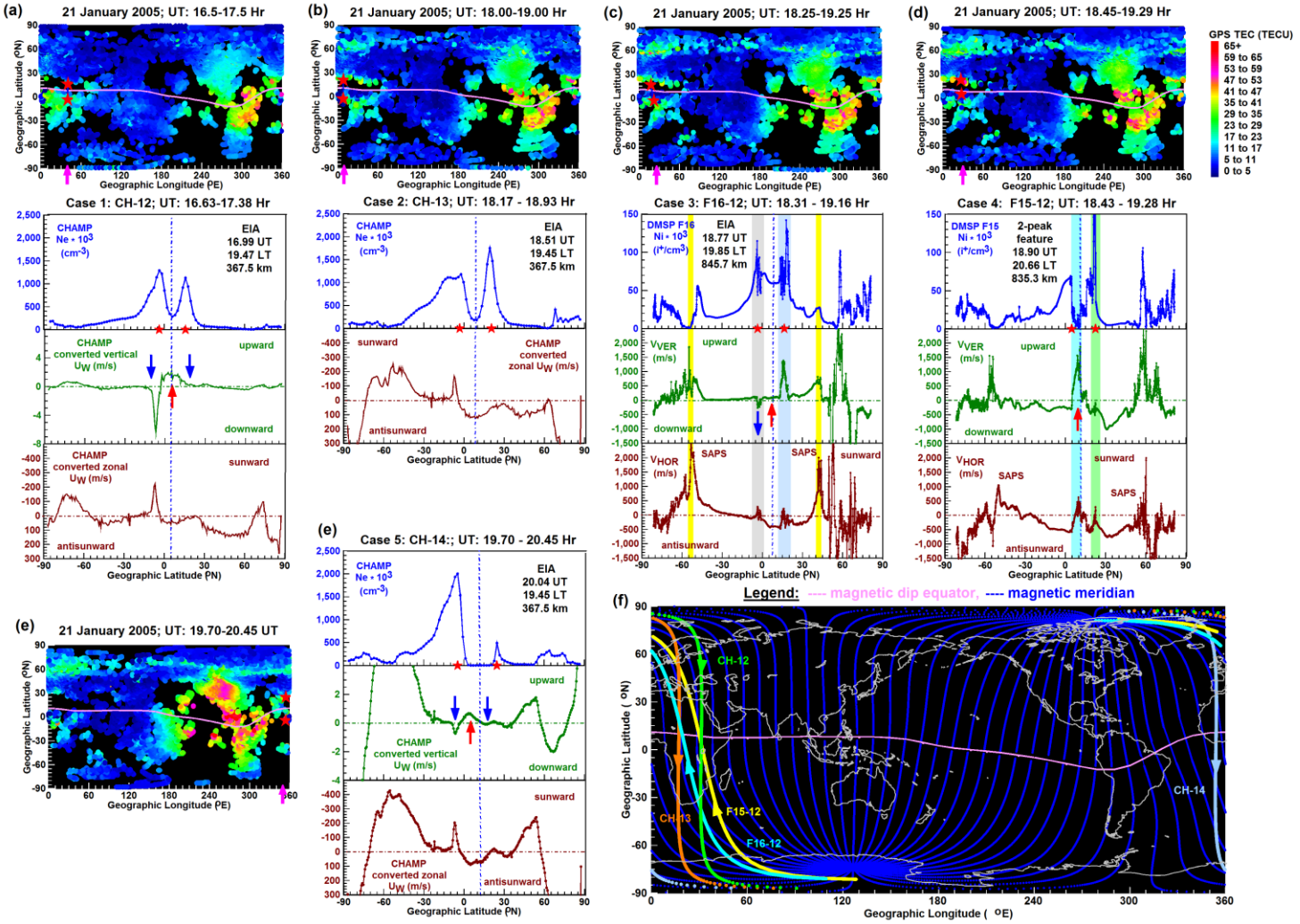

Figure 4: (a)-(e) The GPS TEC maps depict the EIA at the symbol arrow in magenta. (a)-(b) and (e) The CHAMP Ni and wind speed data depict the EIA and underlying plasma fountain respectively and demonstrate the strong M-I-T coupling occurring. (c)-(d) The DMSP Ni and cross-drift data plots depict the supersonic plasma bubbles developed within the distorted EIA. These bubbles drifted upward and westward. (f) The global map shows the ground tracks of the satellite passes utilized.

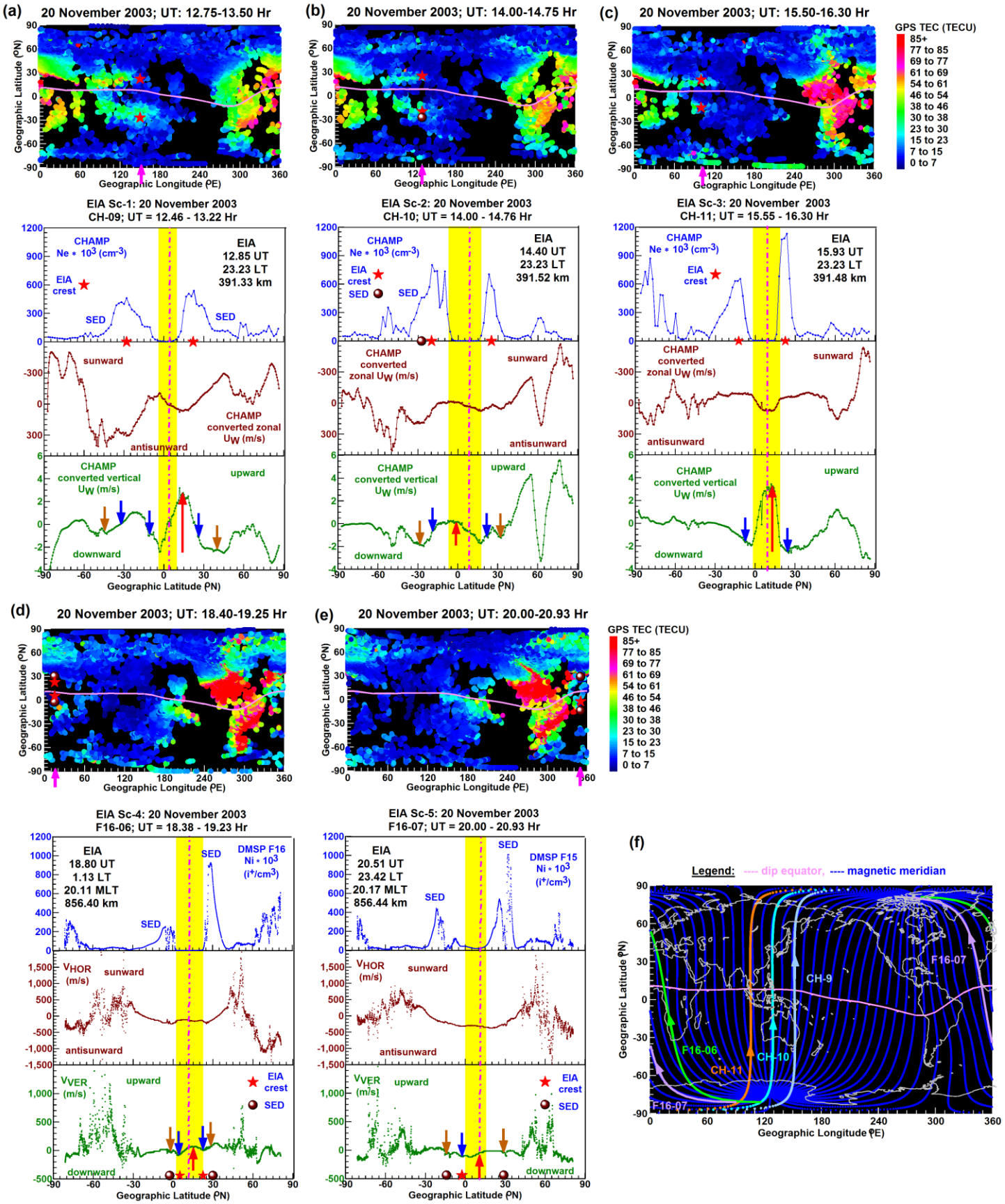

Figure 5: Similar as Figure 4 but constructed for the 20 November 2003 Superstorm to demonstrate strong M-I-T coupling. Then, the feature of storm enhanced density (SED) -appearing poleward of the EIA crest in each hemisphere- was better developed.

We conducted a detailed study of the 20 November 2003 Superstorm in order to further investigate the responses of the coupled M-I-T system at equatorial and subauroral latitudes. This superstorm had been investigated by previous studies (Basu et al., 2007; Mannucci et al., 2008; Zhao et al., 2008) reporting some unusual features. We further investigated some of these unusual features and obtained some new findings that we reported in the journal article of Horvath & Lovell (2021d). Basu et al. (2007) reported the unusual feature of the absence of plasma density depletion (or bite-out or drop-out) detections made earlier than 18.03 UT when the SYM-H index reached its minimum of ~490 nT. With a series of multi-instrument CHAMP line plot sets, we provided observational evidence verifying the detections of the expected plasma density depletions (or drop-outs in Ne detections), occurring soon after the IMF southward turning, at ~12 UT (see Figure 5). The CHAMP observations also depict a large plasma density drop-off in each hemisphere, which is the signature of the plasmapause, and the depletion of the mid- and high-latitude regions poleward of the drop-off. These CHAMP observations provide evidence of the significant role of strong convection E field and SAPS E field in eroding the mid- and high-latitude ionosphere, poleward of the plasmapause.

Our EIA scenarios (Sc-9—Sc-10; see Figure 6) illustrate in each hemisphere a well-developed storm enhanced density (SED; Foster, 1993) feature with a large plasma density drop-off (~$1{,}400\times10^3$ cm^{-3} at ~35°N, geographic, in Sc-10), which is the signature of the plasmapause, and the depleted mid- and high-latitude regions poleward of the drop-off. These observations provide evidence of the significant role of strong convection E field and SAPS E field in eroding the mid- and high-latitude ionosphere, poleward of the plasmapause. Thus, the high O/N_2 content and the chemical composition change were not solely responsible for the plasma density depletions observed, as suggested by Verkhoglyadova et al. (2017), since the convection E field and SAPS E field had also significant roles in eroding the mid- and high-latitude regions, poleward of the plasmapause.

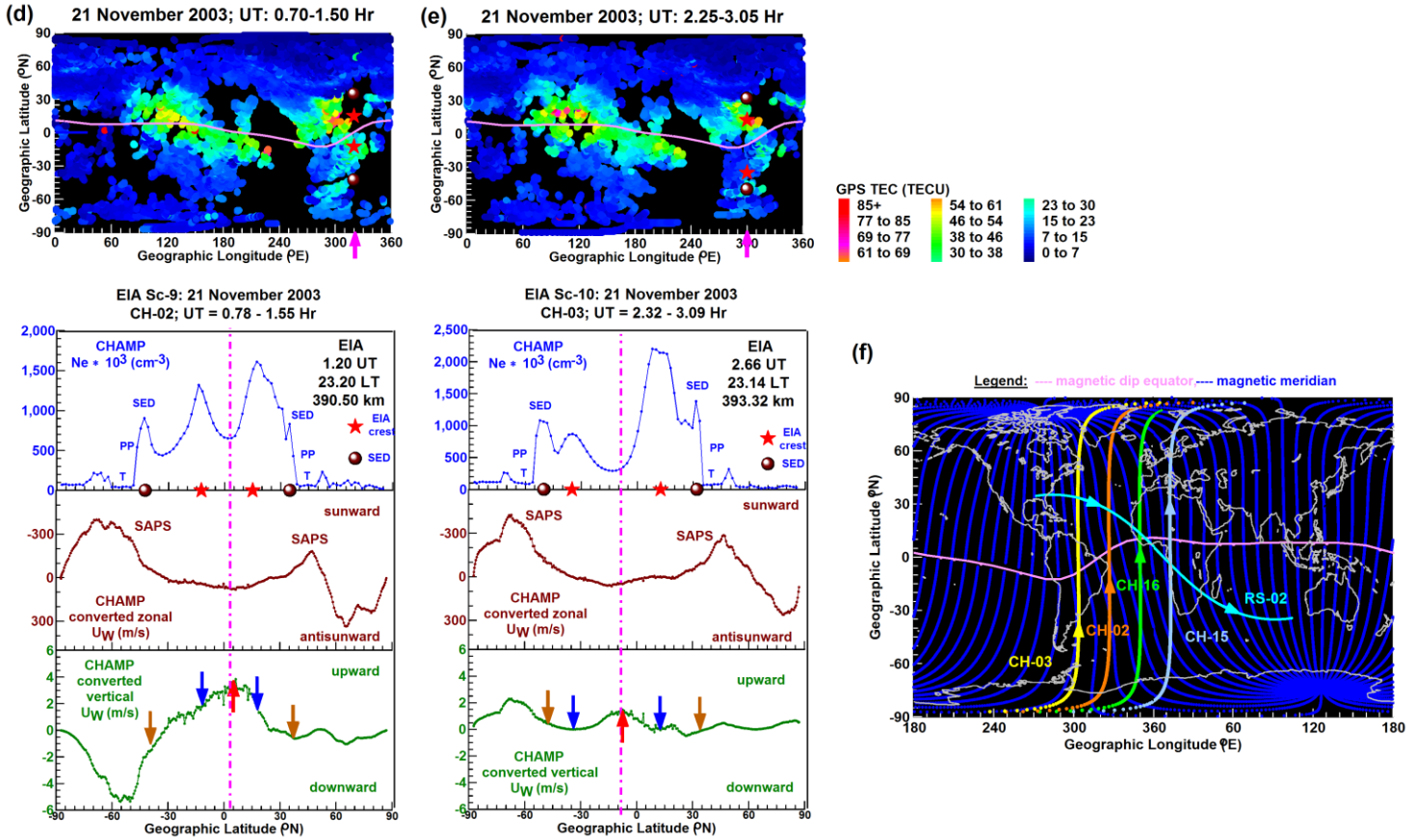

Figure 6: Similar as Figure 5 but depicts the features of plasma density drop-off, which is the signature of the plasmapause (PP), and the low plasma densities poleward of the PP evidencing plasmaspheric erosion.

2.2.3 M-I-T coupling occurring during moderate storms at subauroral latitudes on the duskside

We further investigated the development of complex subauroral flow channels under various magnetic conditions. Covering active conditions, we focused on the strong geomagnetic storm of 27–29 May 2017 and the moderate geomagnetic storm of 16 July 2017 in order to find out how the K-H waves and the K-H instability mechanisms impacted the subauroral and auroral regions. Such impacts were also investigated for the magnetically quiet day of 29 May situated in the recovery phase of the 27-29 May 2017 storm. The new findings of these further investigations are reported in the journal article of Horvath & Lovell (2021c). On 29 May 2017, under magnetically quiet (Kp<3-) and northward IMF conditions, the THEMIS satellite provided an unusually long (~2.5 hours) detection of the K-H surface waves travelling tailward on the dawnside flank of the magnetopause, as previously reported by Lu et al. (2019). As our study shows, the footprint of the THEMIS satellite mapped down to the subauroral region where the impacts of K-H surface waves resulted in the formation of an equatorward-poleward ASAID-SAID flow channel structure earlier and SAPS-ASAID flow channel structure later on (see Figure 7).

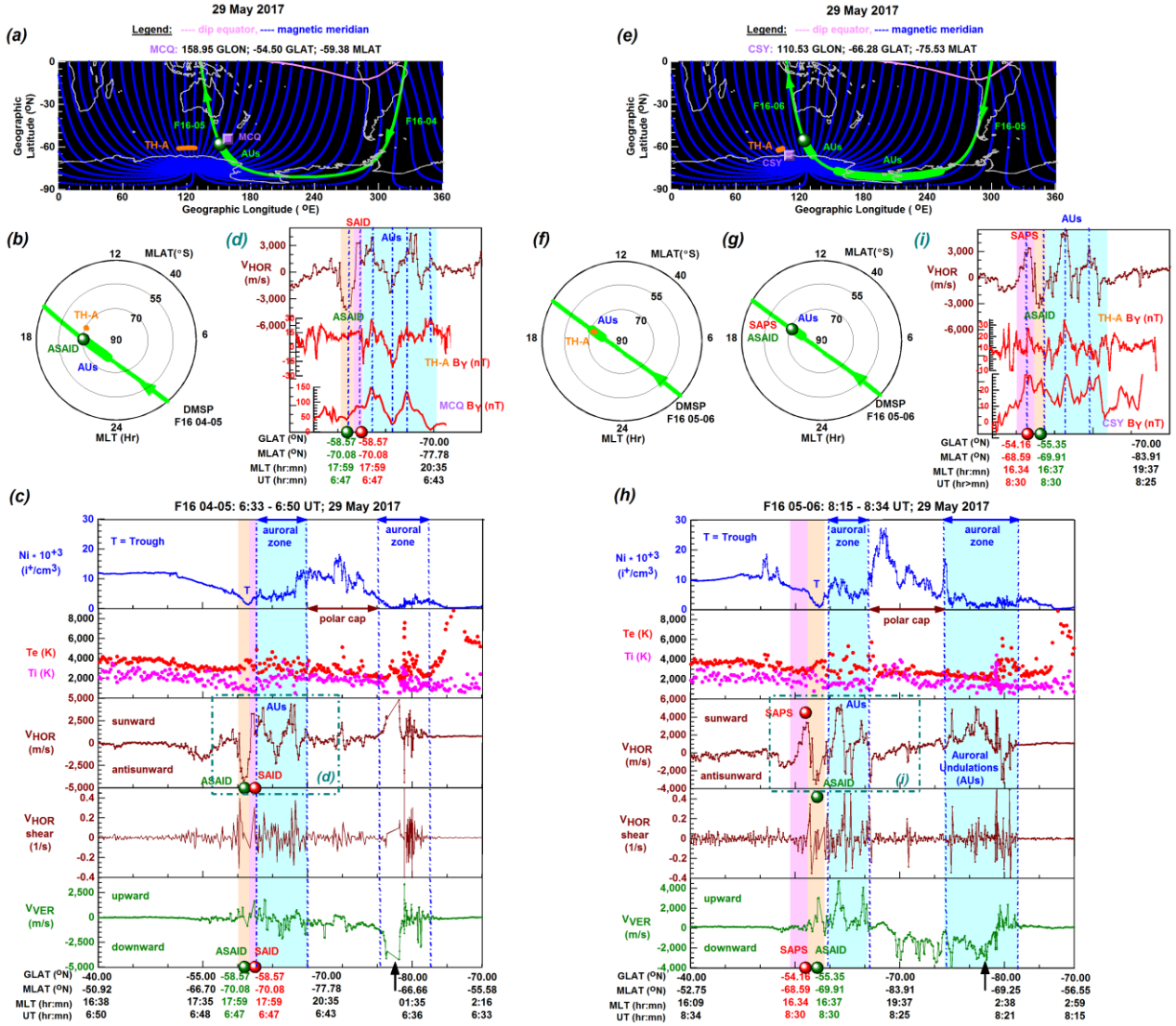

Figure 7: top panel (a) and (e) The southern-hemisphere maps show the ground tracks of satellite providing the observations, the locations of the ASAID feature detected (symbol dot in green), and the sites of the ground-based magnetometer stations (symbol square in purple). middle panel (b)-(d), (f)-(g) and (i) The polar maps show the good correlations of the THEMIS footprints (in orange) tracking K-H waves and the DMSP-detected ASAID (dot in green), SAPS (dot in red) and auroral undulations (AUs; highlighted orbit section). The subsets depict the good correlation found among the subauroral and auroral zonal flows (V_{HOR}), magnetospheric B_Y component measured by THEMIS and geomagnetic B_Y component measured at Macquarie Island (MCQ) or Casey (CSY). bottom panel (c) and (h) The DMSP line plot series depict the complex subauroral flows and the auroral undulations (AUs) and their plasma environment.

On 28 May and 16 July 2017, under southward IMF orientation and storm conditions, the SAPS flows became structured and formed SAPS wave structures (SAPSWS; Mishin et al., 2002), while large auroral undulations occurred inside both the duskside and the dawnside auroral zones (see Figure 8).

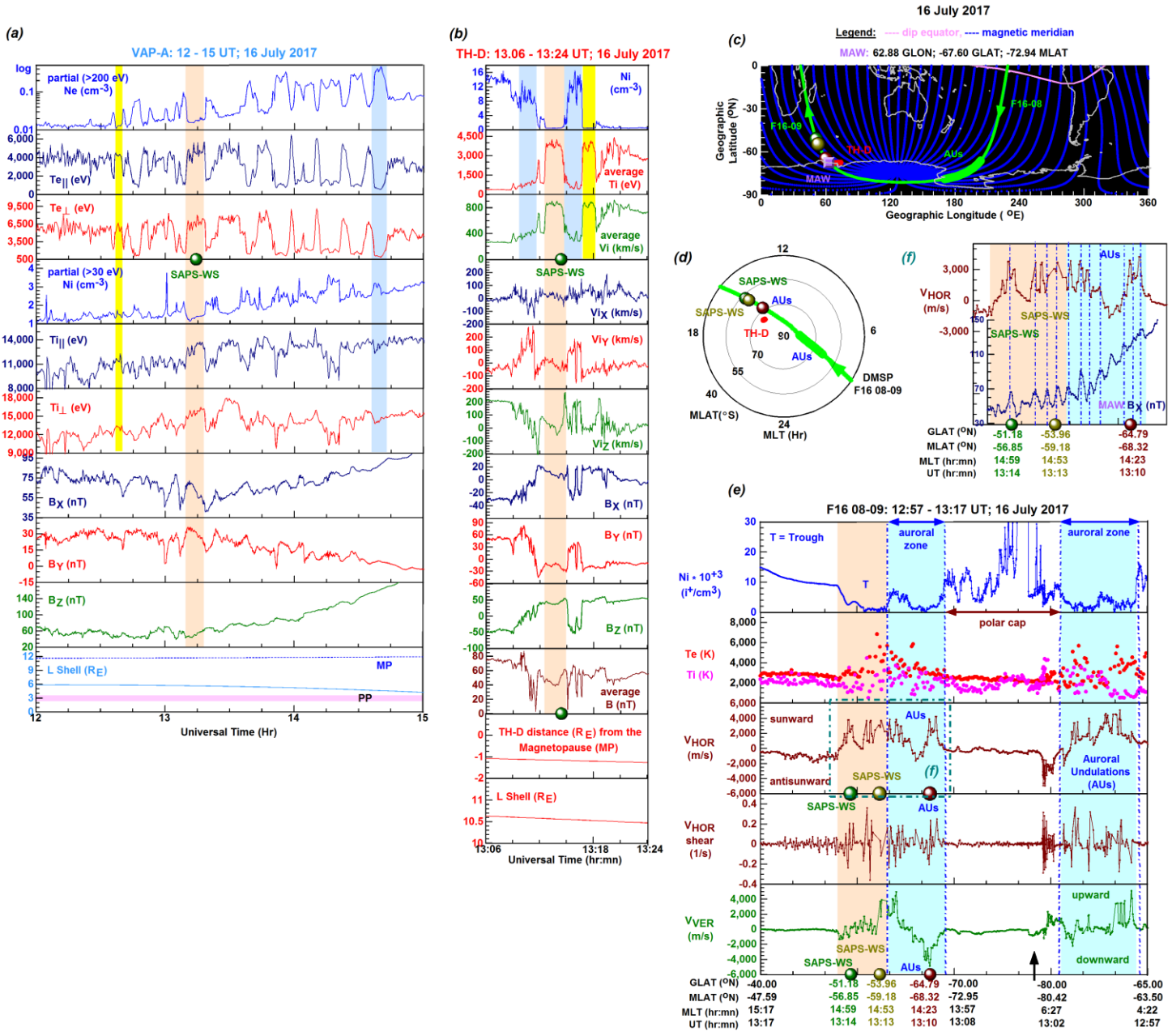

Figure 8: (a) The VAP-A line plot sets depict the hot zone structured by the K-H waves detected by the THEMIS satellite. The time of SAPSWS detection is marked (dot in green; shaded interval in light orange). (b) The THEMIS line plot series depict the K-H waves rolling along the magnetopause. Again, the time of SAPSWS detection is marked (dot in green; shaded interval in light orange). At the point of correlation (i.e. SAPSWS detection marked as dot in green and shaded interval in light orange), the K-H waves structured the hot zone the same way as evidenced by same characteristics: the low Ne and Ni along with the increased Te and Ti. right panel (c)-(f) The same as Figure 7 but constructed for the SAPSWS and nearby auroral undulations. This SAPSWS formed the point of correlation demonstrating the impacts of both the K-H waves and the hot zone on the subauroral and auroral regions.

These correlated observations of the K-H surface waves and subauroral flow channel structures (ASAID-SAID, SAPS-ASAID, SAPSWS) imply that the Near-Earth Plasma Sheet (NEPS; Leonovich & Mazur, 2005) resonator's earthward (inner) boundary became undulating when the NEPS resonator became activated by the K-H waves (Mazur & Leonovich, 2006). To confirm this, we provided observational evidence with VAP-A observations illustrating the structured plasma

sheet plasma and temperature on 28 May 2017 and the surface waves on 16 July 2017 commonly appearing near the plasmapause, within the NEPS: in the hot zone (see Figure 9).

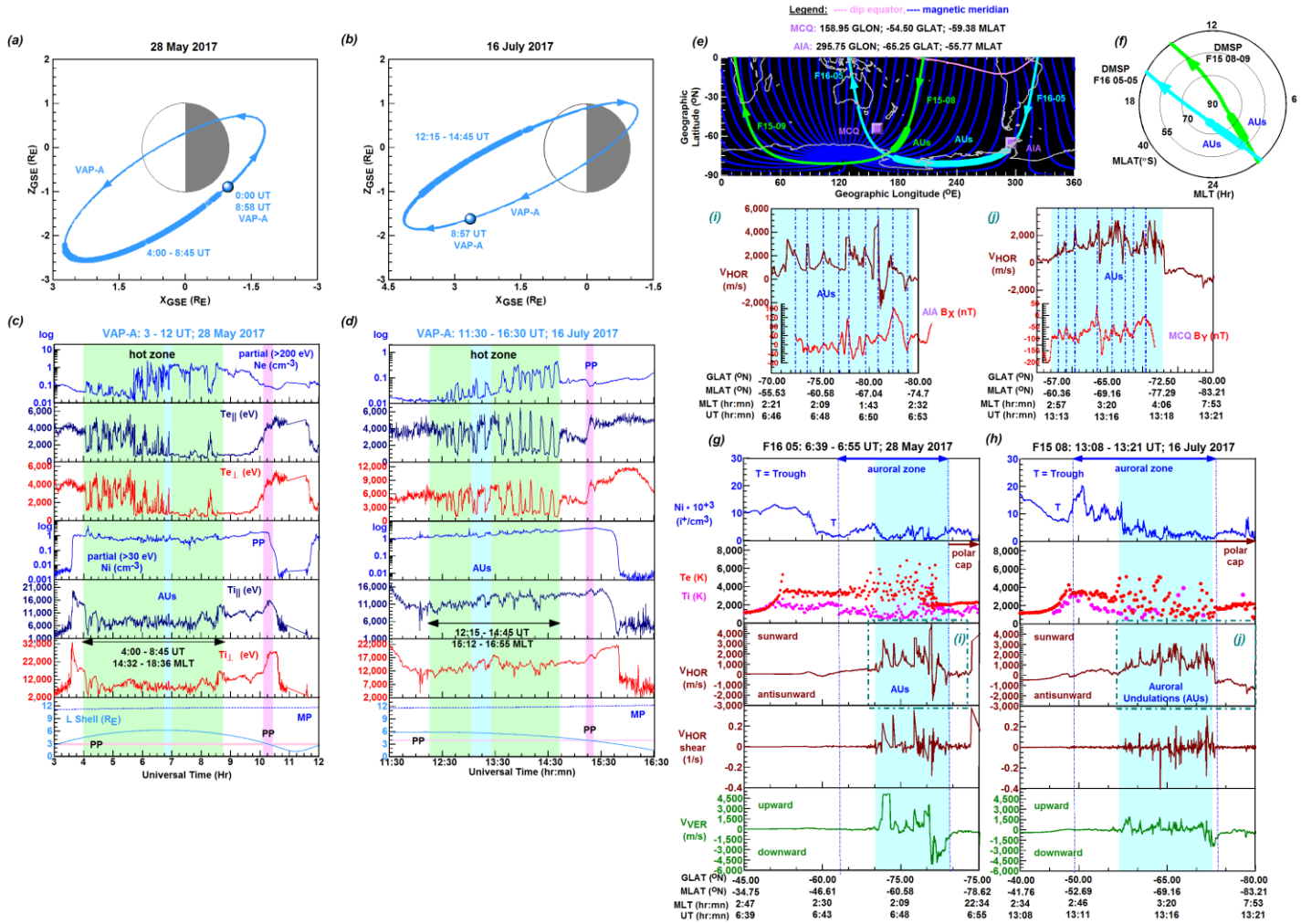

Figure 9: left panel (a)-(b) the orbit plots illustrate the locations of hot zone detections made by the VAP satellite. (c)-(d) The VAP line plots depict the hot zone (shaded interval in light green) during which DMSP detected auroral undulations (shaded interval in cyan). right panel (e)-(j) Similar as Figures 7-8 but constructed for the auroral undulations detected during the hot zone detections made by VAP demonstrating the impacts of both the hot zone and the K-H waves (structuring the hot zone) on the auroral region leading to auroral undulations.

2.2.4 M-I-T coupling occurring during superstorms at subauroral latitudes on the dawnside

We obtained significant results on the dawnside subauroral flows that we reported in the journal article of Horvath & Lovell (2021d). Based on the 20 November 2003 Superstorm duskside SAPS results and the characteristics of the duskside SAPS, we specified the dawnside subauroral flows as dawnside SAPS because of the underlying R2 FACs (see Figure 10c) and because of their northern-hemisphere—southern-hemisphere conjugate nature (see Figure 10b).

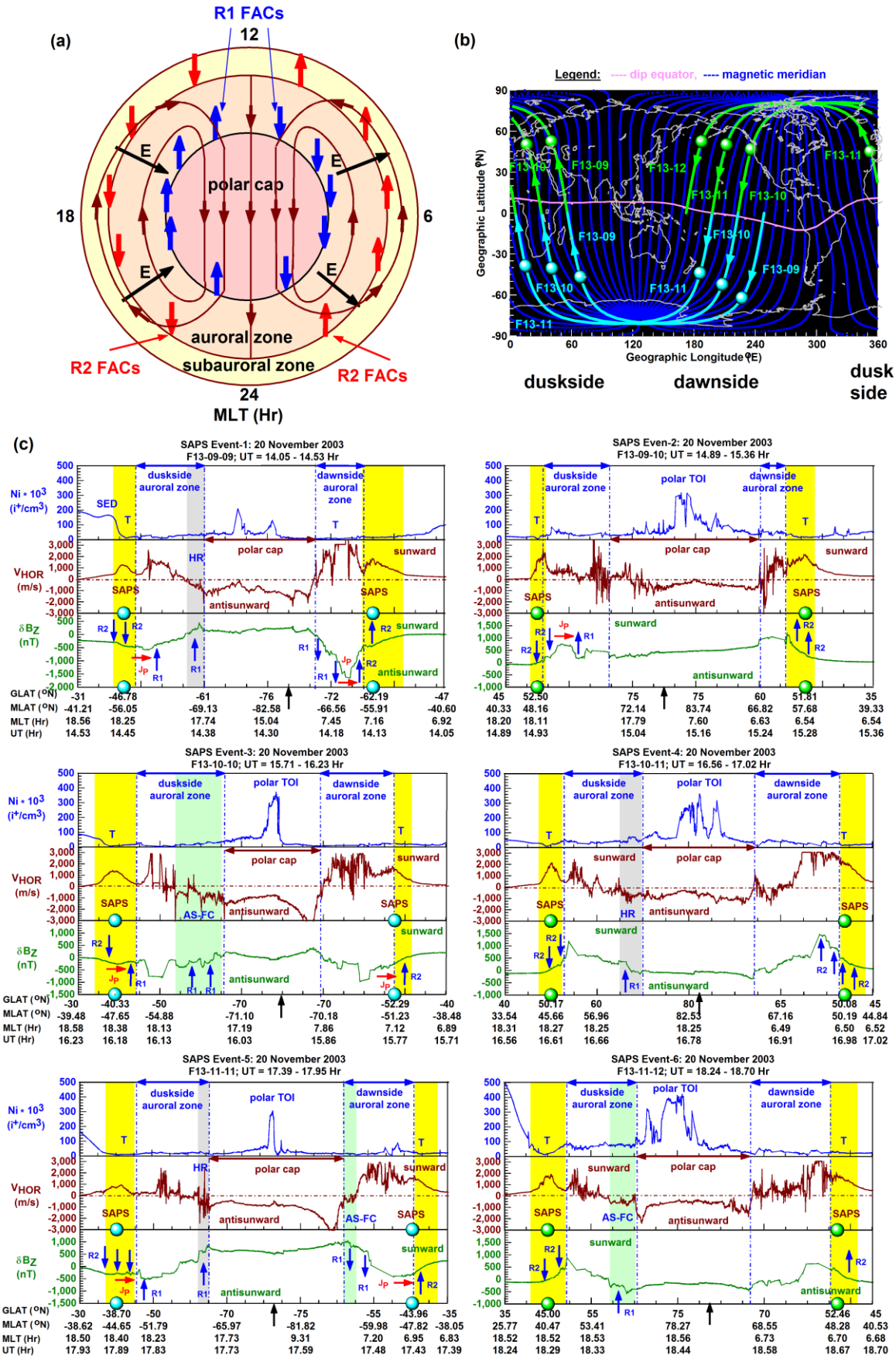

Figure 10: (a) The diagram shows the pattern of the R1 and R2 FACs on the duskside and dawnside in the framework of the two-cell (dusk cell, dawn cell) polar convection. (b) The global map shows the DMSP ascending and descending passes tracking the northern-southern conjugate subauroral flow channels both on the duskside and on the dawnside. (c) The DMSP line plot sets show duskside-dawnside SAPS detections (shaded interval in yellow) and their underlying R2 FACs.

With correlated DMSP-ROCSAT dawnside observations, we demonstrated other important characteristics of the dawnside SAPS (see Figure 11).

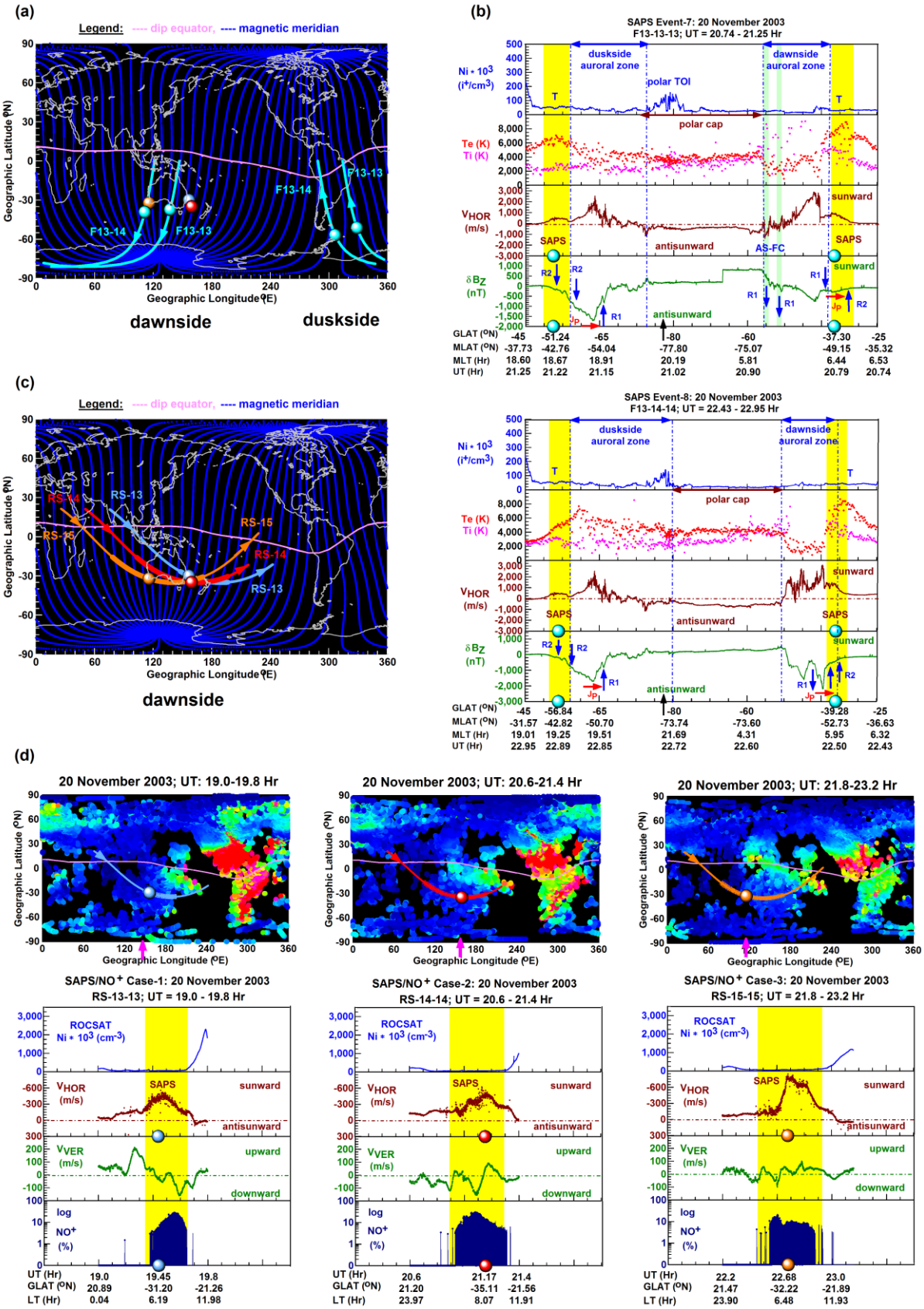

Figure 11: (a) The global map shows the DMSP passes tracking the SAPS flows on the duskside and dawnside. (b) The DMSP line plot sets show the plasma environment of the duskside and dawnside SAPS. (c) The global map illustrates the correlated dawnside DMSP and ROCSAT passes and dawnside SAPS locations. (d) The GPS TEC maps depict the low TEC regions where the dawnside SAPS were detected. The ROCSAT line plot sets depict the low Ni region within the dawnside SAPS, the dawnside SAPS along with the underlying vertical drifts and suddenly enhanced NO^+ content.

These characteristics include the dawnside SAPS' ability to deplete the plasma density due to the underlying high temperature (Te≈8,000 K; Ti≈6,000 K) environment (observed by DMSP; see Figure 11b) that affected the chemical makeup (Mishin et al., 2004) and that was ideal for the quick charge exchange reaction of $N_2 + O^+ \rightarrow NO^+ + N_2$ to occur: a) decreasing the O^+ content and deepening the trough by depleting the plasma densities and b) increasing the NO^+ content (observed by ROCSAT; see Figure 11d).

2.2.5 M-I-T coupling occurring during magnetic quietness at subauroral latitudes on the dawnside

We obtained significant results on the dawnside subauroral flows that we reported in the manuscript of Horvath & Lovell (2021e) submitted to JGR Space Physics that is now under review. In the last study of this project, we also investigated dawnside subauroral flows that developed during magnetically quiet conditions and under northward IMF orientation, when the solar wind was highly Alfvenic (see Figures 12b-c) and unshielded penetration electric field (PEF) impacted the duskside SAPS and led to the development of dawnside subauroral flows (see Figure 12e).

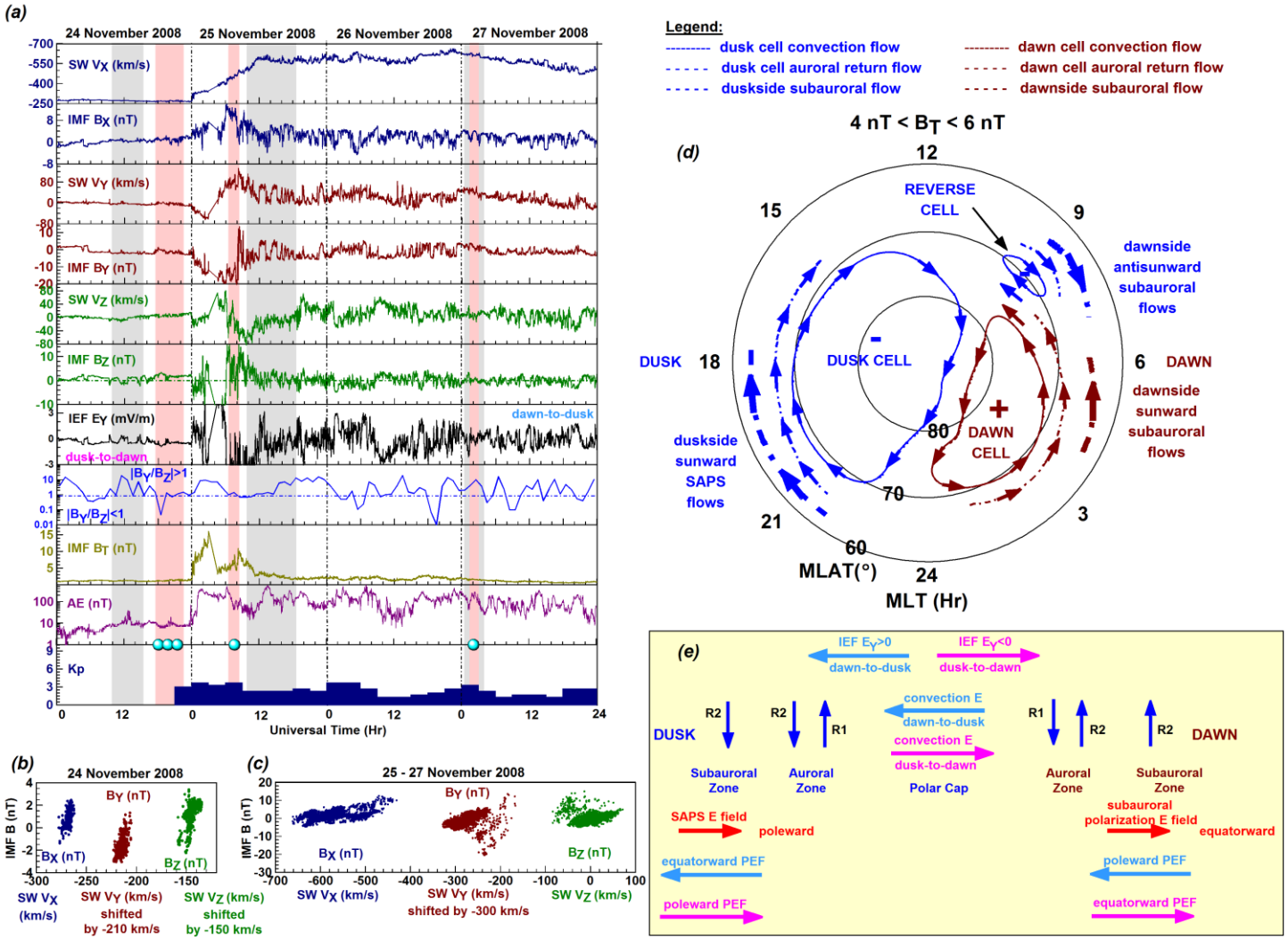

Figure 12: (a) The time series depict the solar wind, IMF, and geomagnetic conditions during the time period investigated. The universal times of dawnside subauroral flow channel detections are marked as symbol dots in cyan and shaded intervals in light red. (b)-(c) The scatter plots show the close correlation of the solar wind and IMF implying antisunward propagating solar-wind Alfven waves. (d) The schematic diagram shows the three-cell (dusk cell, dawn cell, reverse cell) convection pattern operating during the subauroral flow channel detections. (e) The diagram illustrates the various E fields impacting the duskside and dawnside subauroral region.

Under these conditions, a net equatorward directed E field (i.e. polarization E field + unshielded penetration E field) drove the E×B drift eastward in the dawnside subauroral flow channel. But

the dawnside subauroral flows streamed sunward along the dawn cell (see Figure 12d and Figure 13d) and antisunward along the reverse cell (see Figure 12d and Figure 13c). On the duskside, the westward SAPS flows streamed sunward along the dusk cell and became impacted by the unshielded penetration E field (see Figure 12d and Figure 13c).

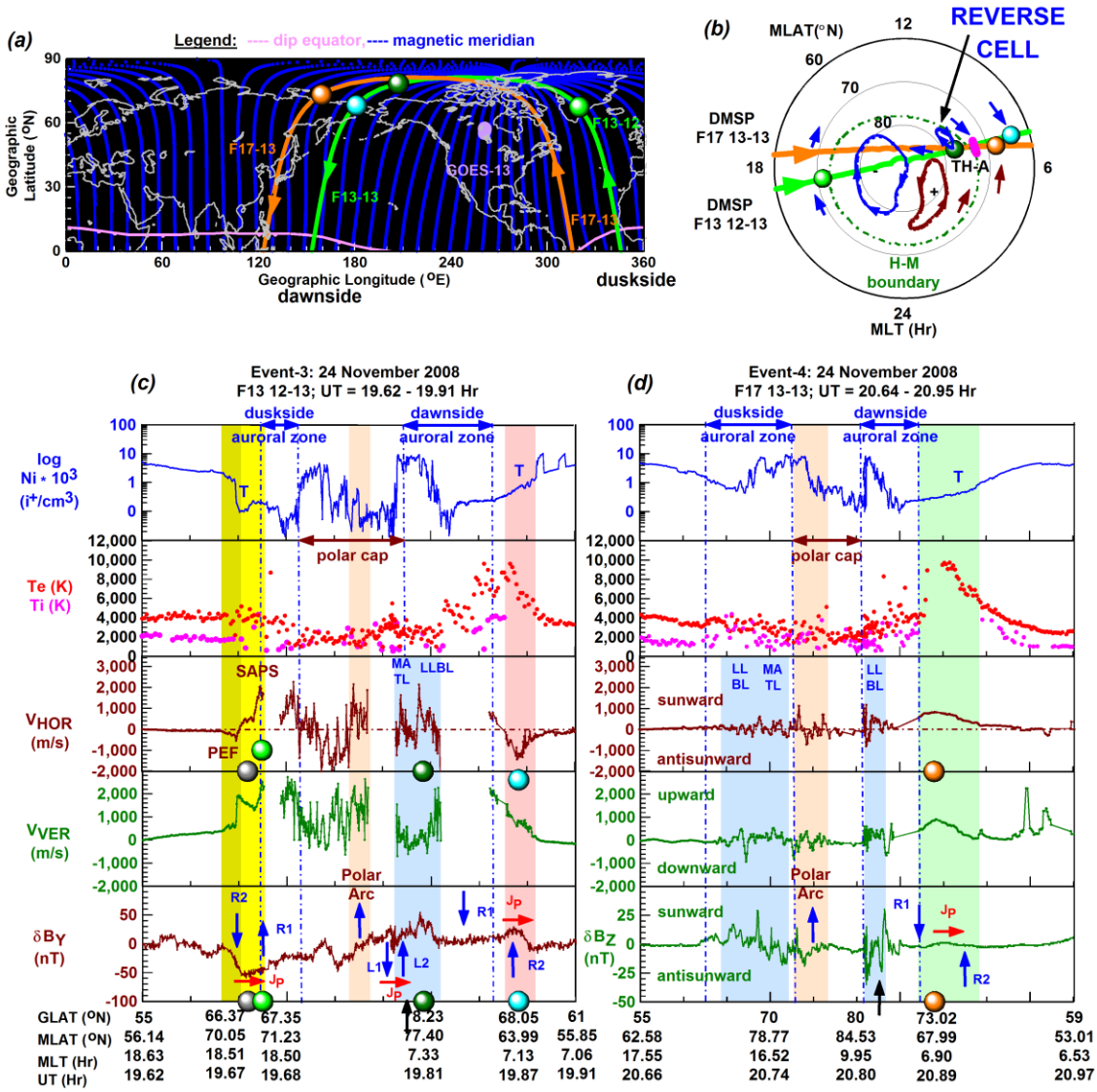

Figure 13: (a)-(b) The maps depict the DMSP passes providing the observations and the locations of the subauroral flow channels along with the three-cell (dusk cell, dawn cell, reverse cell) convection pattern. The DMSP line plot sets show (c) the signature of the unshielded penetration E field (PEF) appearing as an antisunward flow channel, the duskside SAPS impacted by the PEF, and the dawnside eastward subauroral flows streaming antisunward along the reverse cell and (d) sunward along the dawn cell.

2.2.6 Future follow-on project:

Our follow-on project is focused on instability mechanisms including the K-H instability mechanism and the closely related R-T or interchange instability mechanism. These are also closely related and significantly impact the hot zone that is regarded as the most important region of interest for understanding the development and maintenance of various subauroral flows (Mishin & Streltsov, 2021). These include the SAID, SAPS, SAPS wave structures (SAPSWS), Abnormal SAID (ASAID), and Double-peak SAID (DSAID). Since the onsets of various significant satellite missions, detailed investigations of the R-T and K-H instability mechanisms and the hot zone became recently possible. Our major goal is to understand 1) how the hot zone becomes structured or impacted by these instabilities under magnetically quiet and active conditions and 2) what sort of subauroral flows, auroral forms, and polar features develop due to these impacts and 3) what are the underlying driver mechanisms.

References:

Basu, S., Rich, F.J., Groves, K. M., MacKenzie, E., Coker, C., Sahai, Y., Fagundes, P. R., & Becker-Guedes, F. (2007). Response of the equatorial ionosphere at dusk to penetration electric fields during intense magnetic storms. *Journal of Geophysical Research, 112(A8)*, A08308. https://doi.org/10.1029/2006JA012192

Foster, J. C. (1993). Storm time plasma transport at middle and high latitudes. *Journal of Geophysical Research, 98(A2)*, 1675–1689. https://doi.org/10.1029/92JA02032

Foster, J. C., & Burke, W. J. (2002). SAPS: A new categorization for sub-auroral electric fields. *Eos, Transactions American Geophysical Union, 83(36)*, 393–394. https://doi.org/10.1029/2002EO000289

He, F., Zhang, X.-X., Wang, W., & Chen, B. (2016). Double-peak subauroral ion drifts (DSAIDs). *Geophysical Research Letters, 43(11)*, 5554-5562. https://doi.org/10.1002/2016GL069133

Horvath, I., & Lovell, B. C. (2019a). Investigating the development of abnormal subauroral ion drifts (ASAID) during the magnetically quiet times of October 2003. *Journal of Geophysical Research: Space Physics, 124(1)*, 715-733. https://doi.org/10.1029/2018JA026230

Horvath, I., & Lovell, B. C. (2019b). Abnormal subauroral ion drifts (ASAID) and Pi2s during cross-tail current disruptions observed by Polar on the magnetically quiet days of October 2003. *Journal of Geophysical Research: Space Physics, 124(7)*, 6097-6116. https://doi.org/10.1029/2019JA026725

Horvath, I., & Lovell, B. C. (2021a). Complex sub-auroral flow channel structure formed by double-peak sub-auroral ion drifts (DSAID) and abnormal sub-auroral ion drifts (ASAID). *Journal of Geophysical Research: Space Physics, 126*, e2020JA028475 https://doi.org/10.1029/2020JA028475

Horvath, I., & Lovell, B. C. (2021b). Magnetosphere-ionosphere-thermosphere (M-I-T) coupling leading to equatorial upward and westward drifting supersonic plasma bubble development and amplified subauroral polarization streams (SAPS) during the January 21, 2005 moderate storm. *Journal of Geophysical Research: Space Physics, 126*, e2020JA028548. https://doi.org/10.1029/2020JA028548

Horvath, I., & Lovell, B. C. (2021c). Subauroral flow channel structures and auroral undulations triggered by Kelvin-Helmholtz waves. *Journal of Geophysical Research: Space Physics, 126*, e2021JA029144. https://doi.org/10.1029/2021JA029144

Horvath, I., & Lovell, B. C. (2021d). Investigating the coupled magnetosphere-ionosphere-thermosphere (M-I-T) system's responses to the 20 November 2003 Superstorm. *Journal of Geophysical Research: Space Physics, 126*, e2021JA029215. https://doi.org/10.1029/2021JA029215

Kozyra, J. U., Liemohn, M. W., Cattell, C., De Zeeuw, D., Escoubet, C. P., Evans, D. S., et al (2014). Solar filament impact on 21 January 2005: Geospace consequences, *Journal of Geophysical Research. Space Physics, 119(7)*, 5401-5448. https://doi.org/10.1002/2013JA019748

Leonovich, A. S., & Mazur, V. A. (2005). Letter to the Editor: Why do ultra-low-frequency MHD oscillations with a discrete spectrum exist in the magnetosphere? *Annales Geophysicae, 23*, 1075–1079. https://doi.org/10.5194/angeo-23-1075-2005

Lu, S. W., Wang, C., Li, W. Y., Tang, B. B., Torbert, R. B., Giles, B. L., et al. (2019). Prolonged Kelvin–Helmholtz Waves at Dawn and Dusk Flank Magnetopause: Simultaneous Observations by MMS and THEMIS. The Astrophysical Journal, 875(1), 57. https://doi.org/10.3847/1538-4357/ab0e76

Mannucci, A. J., Tsurutani, B. T., Abdu, M. A., Gonzalez, W. D., Komjathy, A., Echer, E., Iijima, B. A., Crowley, G., & Anderson, D. (2008). Superposed epoch analysis of the dayside ionospheric response to four intense geomagnetic storms. *Journal of Geophysical Research, 113(A3)*, https://doi.org/10.1029/2007JA012732

Maurice, S., Thomsen, M. F., Mccomas, D. J., & Elphic, R. C. (1998). Quiet time densities of hot ions at geosynchronous orbit. *Journal of Geophysical Research, 103(A8)*, 17571-17585.

https://doi.org/10.1029/98JA00291
Mazur, V. A., & Leonovich, A. S. (2006). ULF hydromagnetic oscillations with the discrete spectrum as eigenmodes of MHD-resonator in the near-Earth part of the plasma sheet. *Annales Geophysicae, 24*, 1639-1648. https://doi.org/10.5194/angeo-24-1639-2006
Maynard, N. C., Burke, W. J., Basinska, E. M., Erickson, G. M., Hughes, W. J., Singer, H. J., et al. (1996). Dynamics of the inner magnetosphere near times of substorm onsets. *Journal of Geophysical Research, 101(A4),* 7705-7736. https://doi.org/10.1029/95JA03856
Mishin, E. V., Foster, J. C., Potekhin, A. P., Rich, F. J., Schlegel, K., Yumoto, K., et al. (2002). Global ULF disturbances during a stormtime substorm on 25 September 1998. *Journal of Geophysical Research, 107(A12)*, 1486. https://doi.org/10.1029/2002JA009302
Mishin, E., Burke, W., & Viggiano, A. (2004). Stormtime subauroral density troughs: Ion-molecule kinetics effects. *Journal of Geophysical Research, 109(A10)*, A10301. https://doi.org/10.1029/2004JA010438
Sotnikov, V., Kim, T, Mishin, E., Paraschiv, I., & Rose, D. (2015). Sub-Auroral Ion Drifts as a source of Mid-Latitude Plasma Density Irregularities. Proceedings of the Advanced Maui Optical and Space Surveillance Technologies Conference, held in Wailea, Maui, Hawaii, September 15-18, 2014, Ed.: S. Ryan, The Maui Economic Development Board, id.41. https://ui.adsabs.harvard.edu/abs/2015amos.confE..41S/abstract
Verkhoglyadova, O. P., Komjathy, A., Mannucci, A. J., Mlynczak, M. G., Hunt, L. A., & Paxton, L. J. (2017). Revisiting ionosphere-thermosphere responses to solar wind driving in superstorms of November 2003 and 2004. *Journal of Geophysical Research: Space Physics, 122(10),* 10,824–10,850. https://doi.org/10.1002/2017JA024542
Voiculescu, M., & Roth, M. (2008). Eastward sub-auroral ion drifts or ASAID. *Annales Geophysicae, 26(7),* 1955-1963. https://doi.org/10.5194/angeo-26-1955-2008
Wei, D., Yu, Y., & He, F. (2019). The magnetospheric driving source of double-peak subauroral ion drifts: Double ring current pressure peaks. *Geophysical Research Letters*, *46*, 7079–7087. https://doi.org/10.1029/2019GL083186
Zhao, B., et al. (2008). Ionosphere disturbances observed throughout Southeast Asia of the superstorm of 20–22 November 2003. *Journal of Geophysical Research, 113(A3)*, A00A04. https://doi:10.1029/2008JA013054

2.3 How were the results disseminated to communities of interest?

All the major results of this project are documented in journal articles published by the Journal of Geophysical Research Space Physics. The PI had regular communications and active email interactions with Dr. E. V. Mishin (AFRL/RVBXI) throughout the project.

3. Impacts

Demonstrating the significance of the results obtained and the contribution of these new results to the community knowledge base, one of the published articles (Horvath & Lovell, 2021c) was highlighted by UCLA's News and Events (http://themis.igpp.ucla.edu/newsbeta.shtml) and was also featured as an Editor's Highlight in the recently published Eos Science News (https://eos.org/editor-highlights/satellite-data-reveal-magnetospause-k-h-waves-impact-auroras)

4. Changes

4.1 Changes in approach

There were no changes in approach.

4.2 Problems or delays

Manuscript reviewing processes and journal publications were delayed.

4.3 Expenditure Impacts

N/A

4.4 Significant changes in the use or care of human subjects, vertebrate animals and/or biohazards

N/A

4.5 Changes to the primary place of performance from that originally proposed

N/A

5. Technical Updates

The PI had regular email contact with the AOARD Program Manager, Dr. Tony Kim. The PI reported regularly throughout the project the progress made, the new results obtained, and some new ideas on follow up work. Throughout the project, the PI sent updates on manuscript submissions and their publications.